LBL-11323 c.2

Lawrence Berkeley Laboratory
UNIVERSITY OF CALIFORNIA

ENERGY & ENVIRONMENT DIVISION

To be presented at the Western States Section of The Combustion Institute Fall 1980 Meeting, University of Southern California, Los Angeles, CA, October 20-21, 1980. Paper No. WSS/CI-80-45

DETECTION OF S_2 BY TUNABLE ATOMIC LINE MOLECULAR SPECTROSCOPY

Enrique Cuellar

October 1980

RECEIVED
LAWRENCE
BERKELEY LABORATORY

OCT 24 1980

LIBRARY AND
DOCUMENTS SECTION

TWO-WEEK LOAN COPY

This is a Library Circulating Copy which may be borrowed for two weeks. For a personal retention copy, call Tech. Info. Division, Ext. 6782.

LBL-11323 c.2

Prepared for the U.S. Department of Energy under Contract W-7405-ENG-48

DISCLAIMER

This document was prepared as an account of work sponsored by the United States Government. While this document is believed to contain correct information, neither the United States Government nor any agency thereof, nor the Regents of the University of California, nor any of their employees, makes any warranty, express or implied, or assumes any legal responsibility for the accuracy, completeness, or usefulness of any information, apparatus, product, or process disclosed, or represents that its use would not infringe privately owned rights. Reference herein to any specific commercial product, process, or service by its trade name, trademark, manufacturer, or otherwise, does not necessarily constitute or imply its endorsement, recommendation, or favoring by the United States Government or any agency thereof, or the Regents of the University of California. The views and opinions of authors expressed herein do not necessarily state or reflect those of the United States Government or any agency thereof or the Regents of the University of California.

DETECTION OF S_2 BY TUNABLE ATOMIC LINE MOLECULAR SPECTROSCOPY

Enrique Cuellar

Lawrence Berkeley Laboratory
University of California
Berkeley, CA 94720

ABSTRACT

The technique of Tunable Atomic Line Molecular Spectroscopy (TALMS) has been applied to the detection of the molecule S_2. TALMS is a non-intrusive optical technique which promises to be extremely useful in the detection and quantification of small molecules typically present in combustion systems and which exhibit sharp rotational electronic spectra. An atomic emission line which is nearly resonant with a molecular absorption is split into Zeeman components by the application of a magnetic field. It is possible then to magnetically tune one Zeeman component of the atomic emission line into exact resonance with the molecular absorption, while the other unmatched Zeeman component monitors the background. A differential absorption measurement results in a signal which is proportional to the concentration of the molecule of interest.

An atomic transition in the emission spectrum of Cr(I) at 3017.57Å is found to be resonant with a rotational electronic absorption of S_2. By scanning the magnetic field from 0-20 kGauss, it is possible to map out several discrete absorptions of S_2 belonging to the $v' = 7 \leftarrow v'' = 2$ band in the $B^3\Sigma_u^- \leftarrow X^3\Sigma_g^-$ system. These absorptions are identified as branches arising from the triplet splitting of the rotational states of

S_2. This experiment demonstrates the very high specificity of the TALMS technique, as well as the ability to do high resolution spectroscopy of a molecular species by magnetic tuning of the Zeeman components of an atomic emission line.

I. INTRODUCTION

The characterization of emissions produced in the combustion of alternative and fossil fuels play a very important role in the development of energy resources. In this context, the chemistry of the combustion of sulfur containing fuels is of great importance, since sulfur, in the form of organic and inorganic compounds, can account for a significant proportion of the fuel mass. Corrosion in power plants due to sulfuric acid, atmospheric pollution by oxides of sulfur, and acid rain represent enormous problems which can seriously limit the full utilization of fossil fuels.

Sulfur is present in gaseous fuels, fuel oils, and in coal. Gaseous fuels contain sulfur as hydrogen sulfide, and present the least serious environmental problem since they can be scrubbed sulfur-free with better than 99% efficiency [1]. The total sulfur content of heavy oils ranges from 0.5 to 5%, and is principally in the form of thiols, organic sulfides, and thiophenes [1]. Effective hydrodesulfurization processes can significantly reduce the sulfur content of residual fuel oil. In coal, sulfur is bound both in inorganic and organic material, and can account for up to 10% of the coal mass; very little occurs as free sulfur [2]. The principal inorganic form of sulfur in coal is iron disulfide, while organic sulfur is present in coal in the form of heterocyclic rings, the dominant form thought to be thiophene, and in lesser amounts mercaptans, sulfides, and disulfides [3]. Physical

separation methods can remove inorganic sulfur from coal, but organic sulfur can only be removed by drastic chemical treatment.

Much is known about the combustion chemistry of sulfur containing compounds, as indicated in the extensive review by Cullis and Mulcahy [4]. However, a basic mechanistic understanding of all of the decomposition and combustion reactions of relatively simple molecules such as H_2S or CS_2 is not yet available. Furthermore, the combustion kinetics of organic sulfur compounds, such as heterocyclic rings, is virtually unknown. Recent experimental laser fluorescence measurements of fuel rich $H_2/O_2/N_2$ flames with added H_2S have yielded much information about free radical sulfur species in the post flame gases [5]. Such new experimental results, combined with an improved kinetic data base , promise to help clarify the elementary reactions involved in the combustion of sulfur containing compounds.

The principal sulfur containing product formed in the combustion of sulfur compounds is sulfur dioxide (SO_2). Considerable attention has therefore been given to the development of techniques for both ambient air and stationary source SO_2 monitoring. Of these techniques, UV fluorescence methods are clearly recommended for the analysis of SO_2 [6]. These techniques, however, depend on probe sampling of combustion products, and are therefore subject to sampling errors associated with probe effects.

In addition to SO_2, numerous other sulfur containing species are present in flames. Their identification and measurement is clearly of great importance if a detailed kinetic understanding of sulfur chemistry is to be obtained. Equilibrium concentrations of sulfur containing species in hydrocarbon flames have been calculated from thermodynamic data by Johnson et al. [7]. These calculations indicate that SO_2 and SO are the dominant sulfur species present in flame gases. In fuel rich

conditions, however, H_2S, S_2, and SH are also present in significant amounts.

Experimental verification of these calculated equilibrium distributions has been obtained recently by Muller et.al. [5] using the technique of laser fluorescence. These authors report quantitative measurements of the concentrations of species such as SH, S_2, SO, and SO_2 in the post flame gases of fuel rich $H_2/O_2/N_2$ flames containing added H_2S. These results are in qualitative agreement with the calculated concentration profiles of Johnson et. al. [7], and again show that H_2S, S_2, and SH are present in the post flame gases in significant proportions. Laser fluorescence techniques offer the opportunity for making space resolved, optical, non-intrusive measurements of concentrations of species in flames. As such, they do not suffer from the problems associated with probe measurements. However, in order to obtain quantitative information these methods require accurate values for transition probabilities and attention to collisional quenching effects and energy transfer processes.

We present here preliminary results on a new optical technique for measuring concentrations of species such as might be present in a combustion environment. This technique, called Tunable Atomic Line Molecular Spectroscopy (TALMS), is a line of sight, incoherent absorption technique which is highly sensitive and selective. TALMS is based on the Zeeman effect, which allows for magnetic tuning of an atomic line into resonance with a molecular absorption [8]. Atomic absorption spectroscopy based on the Zeeman effect has been used in the analytical determination of numerous atomic species [9], and was recently extended to the detection of small molecules which exhibit sharp rotational electronic structure (e.g. NO [10,11], SO_2 [12]). We have applied

this technique to the detection and measurement of S_2 formed in the equilibrium vapor of elemental sulfur, and from the thermal decomposition of H_2S.

II. EXPERIMENTAL

A. The Zeeman Effect

In the presence of an external magnetic field, atomic energy states which give rise to spectral lines may be split into new states by the Zeeman effect [13]. The interaction of the magnetic field with the magnetic moment of the electrons of the atom generates new energy states whose energies (in cm^{-1}) are given by

$$E = E_o + LgHM_J$$

E_o is the original energy of the atomic state, H is the magnetic induction in gauss, M_J is the magnetic quantum number, and the Lande g factor and Lorentz unit L are given by

$$g = 1 + \frac{J(J+1) + S(S+1) - L(L+1)}{2J(J+1)}$$

where S, L, and J are the spin, orbital, and total angular momentum quantum numbers, respectively, and

$$L = \frac{e}{4\pi mc^2} = 4.67 \times 10^{-2}\ cm^{-1}/kG$$

As an illustration, the normal Zeeman effect in magnesium for the transition at 285.2nm is shown in Figure 1. In the presence of the external magnetic field, the $^1P_1$ upper level of the transition is split

into three components, which are identified by the magnetic quantum number M_J'. Transitions between these new states and the ground state ($M_J'' = 0$) are given by the selection rule:

$$\Delta M_J = 0, \pm 1$$

Transitions with $\Delta M_J = 0$ give rise to the π components of the Zeeman pattern, and are not shifted from the zero-field value ν_o of the transition, while transitions with $\Delta M_J = \pm 1$, called $\sigma\pm$ components, are shifted symmetrically to lower and higher energies about ν_o.

Besides differing in frequency, the π and $\sigma\pm$ components also differ in their polarization, as shown in Figure 2. With transverse observation, that is, observation in a direction perpendicular to the direction of the magnetic field, the π components have their electric vectors linearly polarized parallel to the magnetic field, while the $\sigma\pm$ components have their electric vectors linearly polarized perpendicular to the magnetic field. For longitudinal observation (observation parallel to the magnetic field), π components are not observed, and $\sigma\pm$ components are circularly polarized: the high frequency σ_+ component is circularly polarized in a counterclockwise direction (with the direction of the magnetic field being up from the plane of the figure), while the low frequency $\sigma-$ component is circularly polarized in the opposite direction.

The normal Zeeman effect (The Lorentz triplet) is by no means the general behavior of spectral lines under the influence of a magnetic field. Generally speaking, the Zeeman patterns are much more complicated. For historical reasons [13], these more complex patterns came to be called the "anomalous" Zeeman effect.

B. Tunable Atomic Line Molecular Spectroscopy

The splitting of spectral lines produced by the magnetic field as well as the polarization of these lines form the basis for the detection of molecules by Tunable Atomic Line Molecular Spectroscopy [8-12]. One of the Zeeman components of the atomic emission line is tuned (by varying the strength of the magnetic field) into exact coincidence with a sharp vibrational-rotational transition in the electronic absorption spectrum of the molecule to be detected, while the other component is shifted off resonance. The matching component indicates the extent of absorption by the molecule of interest plus any background absorption due to other species present. The unmatched Zeeman component indicates background absorption only. A differential measurement of the absorption of the matched and unmatched components provides a quantitative measurement of the molecule to be detected.

Absorption and light scattering due to large molecules or small particles (e.g. soot or smoke) coexisting in the absorption region generally do not interfere with the detection of the molecule of interest. UV electronic absorptions of large polyatomic molecules are generally broad [14] (broader than the sharp rotational electronic structure of the small molecules which can be detected by TALMS), and hence would be absorbed equally by both Zeeman components. Similarly, both components of the Zeeman pattern are attenuated equally by scattering from particulates, and hence result in no differential absorption signal.

The restriction that there be a coincidence or near coincidence between an atomic line and a molecular electronic absorption is not as severe as it would first appear. The magnetic field strength required for producing the Zeeman tuning can be obtained with a small electromagnet producing a field of less than 30 kGauss. Since typical line shifts are about 2GHz/kG [13],

magnetic tuning can be achieved over a range of 60 GHz. Furthermore, since there are typically at least four atomic emission lines per Angstrom [15] (at 3000 Å, this corresponds to a line every 80 GHz), it is very likely that an atomic emission line can be found within the Zeeman tunable range of the molecule to be monitored.

A block diagram of the experimental apparatus is shown in Figure 3. The light source (see below) is held between the poles of an electromagnet (Varian model V-4004) which has a hole drilled through one pole to allow for longitudinal observation, parallel to the magnetic field. A small lens was placed in the drilled pole piece to increase the collection of light. The light is focused through a 6 cm quartz cell adapted with a finger containing elemental sulfur (sublimed sulfur, Mallincrodt). The finger is immersed in an oil bath which is heated to T_f = 473K. At this temperature, the vapor pressure of sulfur is about 2 torr, and is composed of the species S_8, S_6, S_4, and S_2 [16,17]. Since the partial pressure of S_2 in this mixture is ~ 1.2×10^{-3} torr, the main body of the cell is heated to T_c = 1023K to insure that all the sulfur vapor is dissociated into S_2 [17].

The variable phase retardation plate [18] consists of a block of fused quartz mounted at a 45 degree angle in a magnetic clamp. The clamp is made from a split laminated transformer core, with a 0.5 mm gap maintained on one side of the clamp by the fused quartz block. The clamp is actuated by a pair of drive coils, and the stress on the quartz block causes an optoelastic effect and produces a retardation of the phase of the light passing through it. By driving the clamp with an a.c. current, a variable retardation effect is produced, which in combination with the fixed linear polarizer in front of the entrance slits of the monochromator, (McPherson

model 218, grating blazed at 2000 Å, 1200 grooves/mm), allows for the alternate transmission of the matched and unmatched Zeeman components of the atomic emission line to the photomultiplier tube (Hamamatsu Type YA7122). The signal is processed electronically and displayed on a strip chart recorder.

The light source is a modification of a magnetically confined arc lamp described by Hadeishi and Anderson [19] is shown in Figure 4. The body of the lamp is made from a one inch stainless steel Varian double-sided Conflat flange. Pole pieces made from permendur or iron are welded to Conflat flange blanks in order to increase the magnetic field strength at the gap. The cathode is made from a stainless steel screw which is hollowed out and packed with the compound or pure metal which gives the desired emission spectrum. The anode is construced from a modified automobile spark plug. Argon gas is flowed through the light source at a pressure of a few torr. A d.c. discharge (30-150 mA) to the cathode results in intense atomic emission, which can be coupled out of the lamp through either a small hole with a suprasil quartz window in one of the pole pieces (for longitudinal observation) or through a window in the main body of the lamp (for transverse observation). The intensity and stability of the atomic emission are adjusted by varying the pressure in the lamp and the strength of the applied current. A machined boron nitride insert and sheet mica discs are used to prevent arcing to the body of the lamp or to the pole pieces.

III. RESULTS AND DISCUSSION

A. Detection of S_2

The electronic spectrum of S_2 has been extensively studied both in absorption and emission [20]. Particular attention has been devoted to the

$B\,^3\Sigma_u^- \leftarrow X\,^3\Sigma_g^-$ system, which extends from 2500 to 7000 Å and contains hundreds of bands which are resolved into rotational electronic transitions. The emission spectrum of chromium was selected as a good candidate for the detection of S_2, principally because there are several intense atomic lines around 3000 Å [21], and the emission spectrum was easy to excite in a reasonably stable manner [22]. Furthermore, SO_2, which is the principal sulfur containing product in the combustion of sulfur compounds (see above) absorbs in the region of 3000 Å [23], and selection of an atomic transition in this region would test the ability to detect S_2 in the presence of SO_2.

Several different cathode materials were used to produce the emission spectrum of chromium, including Cr powder (99%, Fisher Scientific Co.) packed into a hollowed stainless steel screw. Best results are obtained by spot welding several turns of nichrome tape (Tophet C, 16% Cr, 60% Ni and 24% Fe) to the tip of the cathode, and thus exciting the emission spectra of Ni, Cr, and Fe simultaneously. In this manner, relatively stable discharges could be obtained over a period of 2 to 4 hours. The gradual decrease in the intensity of the lamp over this period of time does not affect the measurements since both Zeeman components are equally diminished. Furthermore, by rotating the cathode so that the discharge occurs to a different place on the nichrome tape, the same cathode can be used several times. Periodic cleaning of the lamp housing (by sand blasting) and of the quartz windows is necessary to maintain optimum operating conditions.

The emission spectrum obtained in this manner is shown in Figure 5. The majority of the lines can be readily assigned to these three elements by using the tables of line spectra of the elements given in Reference 21. The richness of the spectrum in the region from 2960 to 3100 Å increases the probability

that a match can be found between an atomic transition and a molecular electronic absorption of S_2.

A higher resolution scan of part of this spectrum is shown in Figure 6. Included are two reference lines from a low pressure Hg lamp. The assignment of the lines was made with the tables given in Reference 21, and the Cr (I) emission line at 3017.57 Å (33,129.6 cm^{-1} vac.) was assigned to the transition $^5D_3 \leftarrow {}^5F_4{}^o$ [24].

Figure 7 shows the differential absorption signal obtained due to the matching of the atomic emission lines with individual S_2 molecular absorptions. The lower trace represents a section of the emission spectrum shown in Figure 5. The upper trace, recorded simultaneously, is the output of the lock-in amplifier. The dotted lines between the two curves show that several atomic emission lines, each one split into its own Zeeman pattern by the external magnetic field, give rise to differential absorption signals corresponding to a match between one of the Zeeman components of each line with a molecular absorption of S_2. Although any one of the matching lines (from Fe or Cr) could be used to detect S_2, we selected the Cr (I) line at 3018 Å because of its higher relative intensity.

B. Magnetic Field Dependence

The dependence of the differential absorption signal due to S_2 on the strength of the external magnetic field is shown in Figure 8. The monochromator was set at 3017.6 Å (100 μ slits) to select the appropriate emission line of Cr (I) and reject stray light. The temperature of the absorption cell (T_c = 1023 K) and of the finger containing elemental sulfur (T_f = 473 K) are maintained constant for each point measurement to make sure that differences in the recorded signal intensity are due to the magnetic field rather than to different concentrations of S_2. Observation is parallel to the magnetic field, so only the

$\sigma+$ and $\sigma-$ components of the Cr atomic line are present. The shift of $\sigma\pm$ components from ν_o is given by

$$\Delta V_s = 0.0438 \text{ cm}^{-1}/\text{kG}$$

As the field is increased from 2.5 kG (a stable discharge could not be maintained at lower field strengths), the signal decreases, and passes through zero at about 8 kG. Increasing the field strength further results in differential absorption signals which are of opposite sign to those obtained at lower fields. This change in polarity implies that at lower field strengths, one of the circularly polarized Zeeman components of the Cr (I) line, $\sigma+$ or $\sigma-$, is in resonance with a molecular absorption of S_2, while at higher fields, this component falls off resonance while the other σ component tunes into a <u>different</u> absorption of S_2. Furthermore, the increasing positive signals observed at the lowest field strengths, where the separation between the $\sigma+$ and $\sigma-$ components is small, suggest that the center of the S_2 absorption which results in this positive signal is very close in frequency to the frequency of the zero field transition of the Cr (I) atomic line at 3018 Å. In order to interpret further the dependence of the S_2 absorption signals on the magnetic field strength, it is necessary to examine both the Zeeman splitting pattern of the Cr (I) atomic transition, as well as the spectroscopy of the $B\,^3\Sigma_u^- - X\,^3\Sigma_g^-$ system of S_2 in more detail.

1. <u>Cr Zeeman Splitting Pattern</u>

The chromium line at 3017. 57 Å is assigned to the transition $3d^4 4s^2 a^5D_3 \leftarrow 3d^4 4s4py\,^5F_4^0$ [24]. The upper $^5F_4{}^0$ and lower $^5D_3$ states are split into 9 and 7 new states respectively by the external magnetic field, as shown in Figure 9. The $\Delta M_J = 0, \pm 1$ selection rule results in a total of 21 allowed transitions in three groups of seven, corresponding to $\sigma-$, π, and $\sigma+$. The Zeeman pattern obtained is an excellent example of the anomalous Zeeman effect, and is shown in Figure 10. Since the separation between individual

lines is almost an order of magnitude smaller than the separation between π and $\sigma\pm$ components, each of the groups of closely spaced $\sigma+$ and $\sigma-$ lines behaves like a single broad component which moves in and out of resonance with the S_2 absorptions as the magnetic field is scanned.

To determine which of these σ components, $\sigma+$ or $\sigma-$, corresponds to the positive and which to the negative S_2 absorption signals observed in Figure 8, the experimental apparatus was modified slightly, as shown in Figure 11. A second linear polarizer is introduced in place of the S_2 absorption cell, and oriented perpendicular to the polarizer in front of the entrance slits of the monochromator. For the purpose of this discussion, assume that the polarizer in front of the monochromator is oriented vertically, in a direction parallel to the slits. The variable phase retardation plate is replaced with a block of fused quartz mounted in a small vise, and oriented such that the stress axis is at 45° relative to the orientation of the linear polarizers. By applying stress to the quartz block, light which is initially linearly polarized becomes circularly polarized. Stress is applied until the intensity of the transmitted light is exactly one half of the intensity transmitted when both linear polarizers are parallel to each other and no stress is applied to the quartz block.

The two orientations of the retardation plate at 90° from each other (Figure 11b) determine whether the transmission of right or left circularly polarized light is favored. With the retardation plate oriented as shown in Figure 11a, (the orientation labeled #1), left circularly polarized light (the $\sigma+$ component of the Cr(I) Zeeman splitting pattern) would be transmitted preferentially, while right circularly polarized light (the

σ- component) would be favored with the retardation plate rotated by 90° (the orientation labeled #2).

The second linear polarizer is then replaced by the S_2 absorption cell (at a fixed temperature), and a 5kG magnetic field is applied to the chromium emission line. The relative intensities I/I_o are measured for both orientations of the retardation plate, and the experiment is then repeated at a field strength of 13 kG. In this manner, it was possible to determine that the positive absorption signal measured at 5 kG (see Figure 8) corresponds to the σ- component of the Cr(I) Zeeman pattern, while the negative signal in Figure 8 corresponds to σ+. At low field strengths, the σ- component is initially in resonance with a sharp electronic absorption of S_2 at about 33,129.6 cm^{-1} (the frequency of the zero field transition of the Cr(I) atomic line). As the field is increased, the σ- component falls off resonance, while the σ+ component falls into resonance with another molecular absorption of S_2, at a higher frequency. The separation between these two absorptions of S_2 can be determined from the separation between the maxima of the positive and negative signals shown in Figure 11, and is estimated to be about 0.56 cm^{-1}.

2. Triplet Splitting of S_2

In order to assign the two observed S_2 absorptions, it is necessary to examine the electronic spectrum of this molecule in more detail. Frequencies for electronic transitions between individual rotational states within each vibrational manifold were calculated using spectroscopic constants given by Huber and Herzberg[25]. As a first approximation, the finer details (due to electronic spin) of the rotational electronic structure of $^3\Sigma$ states were ignored, and the

rotational ladder within each vibrational level was considered to consist of single rotational levels for each value of K, the quantum number for total rotational angular momentum excluding spin. From this initial calculation, the frequency of the Cr(I) transition at 33,129.6 cm^{-1} could overlap with a low K line in the v', v" = 7, 2 band or with a high K (K ~ 60) line in the (4,0) band. Since S_2 is a homonuclear diatomic molecule and the nuclear spin of the ^{32}S nucleus is zero, even numbered K states are missing in the $X^3\Sigma_g^-$ state, and odd numbered K states are missing in the $B^3\Sigma_u^-$ state.

The rotation of the nuclei couples with the motions of the electrons (including spin) in a manner which increases the complexity of the energy level diagram of S_2. The molecular rotation produces a very slight magnetic moment in the direction of $\vec{K}$ (the total rotational angular momentum excluding spin) which causes a slight coupling between $\vec{K}$ and $\vec{S}$ (the electronic spin angular momentum [26]. This coupling, plus the interaction between spins, has the effect that each level given by the quantum number K is split into three levels, F_1, F_2, and F_3, with J = K + 1, K, and K - 1, respectively, where J is the total angular momentum, including spin.

The resulting energy level diagram for a given value of K" in the (7,2) band of S_2 is shown in Figure 12 (for K" = 13). The transitions which are allowed for these triplet split states are also shown. There are six main branches which have $\Delta K = \Delta J$. These are denoted by $R_i(K)$ and $P_i(K)$, where i indexes the F_i levels involved. There are also four weaker satellite branches for which $\Delta K \neq \Delta J$: $^{T}R_{31}$ $^{N}P_{13}$ $^{R}P_{31}$ and $^{P}R_{13}$. In addition to these ten branches, there are also four Q branches, $^{R}Q_{21}$ $^{R}Q_{32}$ $^{P}Q_{12}$ and $^{P}Q_{23}$, but these have not been observed for S_2 [27].

Frequencies for the six main branches and four satellite branches were calculated for K" = 1 to 60 using the expressions for F_1, F_2, and F_3

given in Reference 26. These expressions are functions of two spin splitting constants, γ and λ, which represent a measure of the magnetic field produced by nuclear rotation, and of the magnetic interaction of different spins, respectively. γ and λ are functions of the vibrational quantum number v, and are different for each of the electronic states. Spectroscopic constants for both the $B\,^3\Sigma_u^-$ and $X\,^3\Sigma_g^-$ states were taken from Reference 25, and γ and λ (for v'' = 2) for the ground state from Barrow and Yee [28]. The spin splitting constants for v' = 7 in the excited B state, however, are not well known. Meyer and Crossley [29] reported a value of $\lambda = -4.7$ for the v' = 0, 2, and 4 states, and concluded that v' = 7 is also inverted ($\lambda < 0$) from published data on bands belonging to v' = 7. Barrow and du Parcq [20] reported $\gamma = 0.05$ for v' = 0, 1, and 4.

These two values, $\lambda = -4.7$ and $\gamma = 0.05$, were assumed for v' = 7 and used to calculate the frequencies shown in Table 1. Only those frequencies in the neighborhood of 33,130 cm^{-1} are included for clarity, although the calculation was extended from K''= 1 to 60 [30].

Clearly, the differential absorption signals shown in Figure 8 are due to the overlap of the σ- and σ+ Zeeman components of the chromium atomic line with the rotational branches due to the triplet splitting of $^3\Sigma$ electronic states of S_2. Since a complete experimental rotational analysis (including satellite branches) of the (7,2) band of S_2 is not available, unambiguous assignment of these absorption signals to individual branches of the (7,2) band is difficult. The electronic transitions shown in Table 1 are calculated, and hence subject to errors in the values of the spectroscopic constants, particularly of the spin splitting constants λ and γ [31]. The rotational analyses for other (v',v'') bands of S_2 generally resolve only the main P and

R branches [32], even with the use of high dispersion (~ 0.008 Å/mm) vacuum spectrographs. The weaker satellite branches [33] have been detected only in fluorescence experiments, where a particular v', J' level is selected for excitation [29, 34]. It is remarkable that very high resolution, better that 6×10^4, is possible using the technique of Tunable Atomic Line Molecular Spectroscopy. An additional complication arises from the fact that the σ- and σ+ components which are swept across the S_2 absorptions are themselves quite broad, especially at the higher field strengths. Each component is composed of several closely spaced lines, and the separation between these lines increases with increasing field strength. The absorption signal recorded (see Figure 8) is due to the difference in the absorption of the broad σ- and σ+ components. Thus, overlap of each component with more than one of the closely spaced S_2 absorptions makes full spectroscopic identification of the rotational branches of S_2 difficult.

With these caveats in mind, an interpretation of the magnetic field dependence (Figure 8) is shown in Figure 13. The Cr (I) atomic emission line at 3017.57 Å (33,129.6 cm^{-1} vac.) is nearly resonant with the $P_3(13)$ branch of S_2, calculated at 33,129.7 cm^{-1} (see Table 1). At a field strength of 2 kG, the differential absorption is dominated by the σ- component, resulting in the large positive signal observed in Figure 8. As the field increases, the σ- and σ+ components spread apart, and begin to overlap two other branches of S_2, R_2 (13) and R_1 (21), at 33,129.3 and 33,130.0 cm^{-1} respectively. At ~ 8 kG, the σ- and σ+ components overlap these two branches approximately equally, and hence result in no differential absorption signal Both of the σ components are attenuated equally by <u>different</u> S_2 absorptions. As the field increases to 13 kG, the σ- component moves off resonance from

the $R_2(13)$ branch, while σ+ overlaps the satellite branch ${}^{R}P_{31}(21)$ at 33,130.2 cm^{-1}, resulting in a negative absorption signal. The roles of σ- and σ+ as monitors of S_2 and of background are reversed, and hence the polarity of the observed S_2 differential absorption signal is also reversed. As the field is increased further to 20 KG, the low frequency σ- component remains off resonance with any of the rotational branches of S_2 (the next branch is calculated to be ${}^{N}P_{13}(9)$ at 33,127.9 cm^{-1}), while σ+ begins to overlap ${}^{T}R_{31}(27)$ at 33,130.6 cm^{-1}. This overlap results again in an increasing negative differential absorption signal.

C. Thermal Decomposition of S_2

The results given above show that a Cr (I) atomic emission line at 3018 Å is suitable for the detection of S_2 formed in the equilibrium vapor of solid sulfur. We present now preliminary results in the quantitative measurement of S_2 formed in the thermal decomposition of H_2S.

For this measurement, the sealed off absorption cell shown in Figure 3 is replaced with an open quartz cell 24 cm long and heated to a maximum external temperature of 1050 K. H_2S diluted in H_2 (10%, Matheson Co.) is preheated in a 56 cm quartz side arm ($T_{external}$ = 1300 K) and flows through the absorption cell at a flow rate of 10 to 50 sccm. The exit from the cell is open to the atmosphere. The light source was placed between the poles of a permanent magnet (H = 4.4 kG, see Figure 4b), and the Cr (I) emission was coupled out in a direction perpendicular to the direction of the magnetic field. At a field strength of 4.4 kG, the differential absorption signal observed in this configuration is due to overlap of the π component of the Cr (I) atomic line with the $P_3(13)$ absorption of S_2.

The signal due to S_2 formed by the decomposition of H_2S in H_2 is shown in Figure 14. About two minutes after the gas flow is started, the S_2 signal levels off and remains constant (for constant flow). The temperature of the cell is measured with a thermocouple outside the cell, while the temperature of the gas inside the cell is not known, but assumed to be somewhat lower (see below).

The strength of the differential absorption signal is proportional to the concentration of S_2 in the cell, and can be calibrated against the signals obtained with the 6 cm cell containing elemental sulfur described earlier. This evacuated cell is adapted with a finger containing solid sulfur. With the finger immersed in a heated oil bath, sulfur vapor consisting of an equilibrium mixture of S_2, S_4, S_6, and S_8 [16,17] is formed. By heating the body of the cell to 1023 K, all of the sulfur vapor is dissociated to S_2, with only negligible amounts remaining of S_4, S_6, and S_8 [17]. A correction for line broadening needs to be applied, since the calibration cell is at low pressure (1-2 torr) while the flow cell is nearly at atmospheric pressure. We have not yet measured the broadening correction for S_2 in H_2, but as a first approximation, it is assumed to be similar to that for NO or SO_2 in N_2 [11,12]. With an additional correction for the difference in lengths of the calibration cell and the flow cell, the signal shown in Figure 14 (between points A and B) is estimated to correspond to $\sim$ 50 ppm S_2.

When the flow of the H_2S/H_2 mixture is stopped (point B in Figure 14), the S_2 signal increases dramatically, probably due to increased formation of S_2 by more effective heating of the gas under no-flow conditions. This increase in the S_2 signal strength is shown in Figure 15(b) on a different scale. Eventually, the S_2 signal decreases as the S_2 disappears from the

optical path by reaction or diffusion out of the open cell. Figure 15(a) shows the simultaneous recording of the output of the photomultiplier tube, indicating the extent of absorption by all species present in the heated cell. At the peak of the S_2 absorption signal, only about 25% of the light is transmitted through the cell. Even after the S_2 disappears, the percent transmission remains low, indicating the presence of other absorbing species in the optical path. An UV spectrum of the contents of the cell revealed the presence of SO_2, which also absorbs in the region from 2900 to 3100 Å [23]. The SO_2 is formed by reaction with atmospheric oxygen backstreaming through the open end of the cell when flow is stopped. Clearly, though, the presence of SO_2 does not interfere with the detection of S_2.

IV. CONCLUSIONS

A technique called Tunable Atomic Line Molecular Spectroscopy (TALMS) is described and shown to be suitable for the optical *in situ* detection of small molecules such as may be present in a combustion environment. This technique is based on the splitting of an atomic line into Zeeman components by the presence of an external magnetic field. By varying the strength of the magnetic field, one of the Zeeman components is tuned into resonance with a sharp rotational electronic absorption of the molecule of interest, while the other component is shifted off resonance. A differential measurement of the absorption of the matched and unmatched components provides a quantitative measurement of the molecule to be detected. A Cr(I) atomic emission line at 3017.57 Å is found to be nearly resonant with one of the rotational branches of S_2 which arises due to the triplet splitting of the $B^3\Sigma_u^-$ and $X^3\Sigma_g^-$ electronic states of S_2. By scanning the magnetic field from 0 to 20 kG, both positive and negative differential absorption signals are observed, corresponding to absorption by different rotational branches

of S_2. In this manner, the high resolution capability (greater than 60,000) of the TALMS technique is demonstrated.

This technique is also used to measure the concentration of S_2 formed in the thermal decomposition of H_2S. A value of 50 ppm S_2 is estimated by calibrating against the known concentration of S_2 in the equilibrium vapor of elemental sulfur. The selectivity of the TALMS technique is demonstrated by the ability to detect S_2 in the presence of SO_2.

ACKNOWLEDGEMENTS

The author wishes to thank Tet Hadeishi for many helpful discussions during the course of this work, and is especially grateful to Nancy Brown for her support and friendship. This research was sponsored by the Environmental Office of the U.S. Department of Energy under contract No. W-7405-ENG-48.

REFERENCES

1. W. Strauss, in Air Pollution Control Part I (W. Strauss, ed.), Wiley-Interscience, New York (1971).

2. H.B. Palmer and D.J. Seery, Ann. Rev. Phys. Chem. 24, 235 (1973).

3. P.C. Malte and D.P. Rees, in Pulverized Coal Combustion and Gasification (L.D. Smoot and D.T. Pratt, eds.), Plenum Press, New York (1979).

4. C.F. Cullis and M.F.R. Mulcahy, Comb. and Flame 18, 225 (1972).

5. C.H. Muller III, K. Schofield, M. Steinberg, and H.P. Broida, 17th Symp. (Int.) Combustion, 867 (1979).

6. See for example Instrumentation for Environmental Monitoring, Environmental Instrumentation Group, Lawrence Berkeley Laboratory, University of California, Berkeley (1976).

7. G.M. Johnson, C.J. Mathews, M.Y. Smith, and D.J. Williams, Comb. and Flame 15, 211 (1970).

8. H. Koizumi, T. Hadeishi, and R.D. McLaughlin, Appl. Phys. Lett. 34, 382 (1979).

9. See for example T. Hadeishi and R.D. McLaughlin, Science (London) 174, 404 (1971); H. Koizumi and K. Yasuda, Spectrochim. Acta (Part B) 31B, 237 (1976); ibid., Spectrochim. Acta B 31, 523 (1977); ibid., Anal. Chem. 48, 1178 (1976).

10. H. Koizumi, T. Hadeishi, and R.D. McLaughlin, Appl. Phys. Lett. 34, 277 (1979).

11. ibid., Anal. Chem. 52, 500 (1980).

12. ibid., Anal. Chem. (to be published 1980).

13. E.U. Condon and G.H. Shortley, The Theory of Atomic Spectra, Cambridge University Press, Cambridge (1951).

14. G. Herzberg, Molecular Spectra and Molecular Structure III. Electronic Spectra and Electronic Structure of Polyatomic Molecules, Van Nostrand Reinhold Co., New York (1966).

15. G.R. Harrison, MIT Wavelength Tables, John Wiley and Sons, New York (1939).

16. W.A. West and A.W.C. Menzies, J. Phys. Chem. 33, 1880 (1929).

17. H. Braune, S. Peter, and V. Neveling, Z. Naturforsch. 6a, 32 (1951).

18. B.D. Zak, B. Chang, and T. Hadeishi, Applied Optics 14, 1217 (1975).

19. T. Hadeishi and T. Anderson, Opt. Comm. 23, 252 (1977).

20. R.F. Barrow and R.P. du Parcq, in Elemental Sulfur (Beat Meyer, ed.) John Wiley and Sons, New York (1965), and references cited therein.

21. J. Reader and C.H. Corliss, "Line Spectra of the Elements," Handbook of Chemistry and Physics, 60th edition, CRC Press, Boca Raton, Florida (1979-1980).

22. Atomic transitions from elements other than Cr have been used to excite the UV fluorescence of S_2:Mg (E. Durand, J. Chem. Phys. 8, 46 (1940)); Zn or Cd (K.E. Meyer and D.R. Crosley, Can. J. Phys. 51, 2119 (1973)).

23. W.B. Pearse and A.G. Gaydon, The Identification of Molecular Spectra, John Wiley and Sons, New York (1950).

24. J. Sugar and C. Corliss, J. Phys. Chem. Ref. Data 6, 317 (1977).

25. K.P. Huber and G. Herzberg, Molecular Spectra and Molecular Structure IV. Constants of Diatomic Molecules, Van Nostrand Reinhold Co., New York (1979).

26. G. Herzberg, Molecular Spectra and Molecular Structure I. Spectra of Diatomic Molecules, Van Nostrand Reinhold Co., New York (1950).

27. R.F. Barrow and J.M. Ketteringham, Can. J. Phys. 41, 419 (1963).

28. R.F. Barrow and K.K. Yee, Acta Physica Acad. Sci. Hungaricae 35, 239 (1974).

29. K.A. Meyer and D.R. Crosley, Can. J. Phys. 51, 2119 (1973).

30. A similar calculation was performed for the (4,0) band, but the

calculated frequencies did not match the experimentally determined frequencies for the S_2 absorptions.

31. The large variations in λ' between adjacent vibrational levels in the $B^3\Sigma_u^-$ state is due to mixing by another electronic state. This state is strongly perturbed by the $B''^3\Pi_u$ and $d'\Pi_u$ states (see ref. 20 and 29), making reliable evaluations of λ' and γ' very difficult.

32. See for example S.M. Naudé, South African J. Science 41, 128 (1945); K. Ikenoue, Science of Light 9, 79 (1960).

33. J.B. Tatum and J.K.G. Watson, Can. J. Phys. 49, 2693 (1971).

34. K.K. Yee, R.F. Barrow, and A. Rogstad, J. Chem. Soc. Faraday Trans. 68, 1808 (1972).

TABLE CAPTIONS

Table 1. Calculated values for the rotational branches of S_2 ($B^3\Sigma_u^- - X^3\Sigma_g^-$, v' = 7, v'' = 2). See Text for the spectroscopic constants used. Only the transitions near the value for the Cr (I) line (3017.57 Å (air) or 33,129.6 cm^{-1} (vac)) are included.

CALCULATED S_2 ELECTRONIC TRANSITIONS (cm^{-1})

$B^3\Sigma_u^- - X^3\Sigma_g^-$ v' = 7, v'' = 2

K''	R_1	R_3	R_2	P_1	P_3	P_2	$T_{R_{31}}$	$R_{P_{31}}$	$P_{R_{13}}$	$N_{P_{13}}$
5						33,134.3				33,135.2
7						33,131.3				33,132.0
9			33,135.5		33,138.8	33,127.6			33,134.6	33,127.9
11			33,132.7		33,134.6	33,123.2			33,131.2	33,123.0
13			33,129.3	33,139.7	33,129.7				33,127.0	
15		33,136.7	33,125.2	33,133.8					33,122.1	
17		33,132.1		33,127.2						
19	33 136.3	33,126.8		33,120.0				33,136.9		
21	33,130.0							33,130.2		
23	33,123.1							33,122.9		
25							33,137.5			
27							33,130.6			
29							33,123.1			

FIGURE CAPTIONS

Figure 1. Normal Zeeman effect for the Mg(I) transition at 285.2 nm. $\sigma+$ and $\sigma-$ are shifted symmetrically to higher and lower energies about the unshifted π component. The separation between π and σ components is indicated for a field strength of 10 kG.

Figure 2. Polarization dependence of the π and $\sigma\pm$ Zeeman components. Longitudinal and transverse observation refer to observation parallel and perpendicular to the direction of the magnetic field, respectively. The direction of the magnetic field is up from the plane of the figure.

Figure 3. Schematic diagram of the experimental apparatus (see text).

Figure 4. (a) Light source: magnetically confined arc lamp. The cathode consists of any material which will produce the desired atomic emission spectrum when excited by a d.c. discharge. (b) The configuration used for transverse observation, with the light source held between the poles of a permanent magnet.

Figure 5. Atomic emission spectrum obtained by using nichrome tape (Tophet C, 16% Cr, 60% Ni, and 24% Fe) as cathode material. The arrow points to the Cr (I) line at 3018 Å which was selected for the detection of S_2.

Figure 6. Higher resolution scan of the region around the line indicated by the arrow in Figure 5. Two lines from a low pressure Hg lamp are superimposed on the nichrome spectrum as aids in the assignment.

Figure 7. The lower trace is a scan of the emission spectrum of nichrome tape. The upper trace monitors the differential absorption signals due to matching of the Zeeman split atomic emission lines with different molecular absorptions of S_2 (see text). The temperatures of the S_2 absorption cell are T_f = 473K, T_c = 1023K. H = 5kG. Care must be taken to distinguish true differential absorption signals from excursions of the lock-in amplifier when the light intensity is near zero.

Figure 8. Differential absorption signal due to S_2 as a function of the strength of the external magnetic field. $\Delta V_s = 0.0438\ cm^{-1}/kG$.

Figure 9. Splitting of the $^5F_4{}^0$ and $^5D_3$ levels of chromium by the external magnetic field. Transitions between the new energy levels are given by the selection rule $\Delta M_J = 0, \pm 1$.

Figure 10. Zeeman splitting pattern for the Cr(I) line at 3017.57 Å. Each of the π and $\sigma\pm$ components consists of seven closely spaced lines. The separations between these lines and between the Zeeman components depend on the magnetic field strength, and are indicated for a field of 10 kG.

Figure 11. Experimental determination of which σ component (σ+ or σ-) results in which differential absorption signal of S_2 (positive or negative).

Figure 12. Triplet splitting of the rotational levels of S_2. The v"=2 level is normal while the v'=7 level is inverted. The six main branches ($\Delta K = \Delta J$) and four satellite branches ($\Delta K \neq \Delta J$) are shown for K" = 13. The Cr (I) emission line overlaps the $P_3(13)$ line.

Figure 13. Interpretation of the differential absorption signal for S_2 as a function of increasing magnetic field (see text).

Figure 14. Signal due to S_2 formed by the decomposition of H_2S. The flow of gas (10% H_2S in H_2) is started at point A (time constant = 25 s). At point B, the flow is stopped. The dramatic increase in the signal when the flow ceases is believed to be due to the increasing gas temperature. The temperature of the quartz cell measured externally is 1033 K.

Figure 15. (a) Percent transmission through the absorption cell (left ordinate). The low %T even after the S_2 disappears is due to the presence of SO_2.

(b) Differential absorption signal due to S_2 (right ordinate) The flow of H_2S in H_2 (10%) through the heated cell (Texternal = 973K) is stopped at time t = 0. The S_2 signal increases as the gas heats up, then decays as S_2 disappears by reaction or diffusion out of the cell.

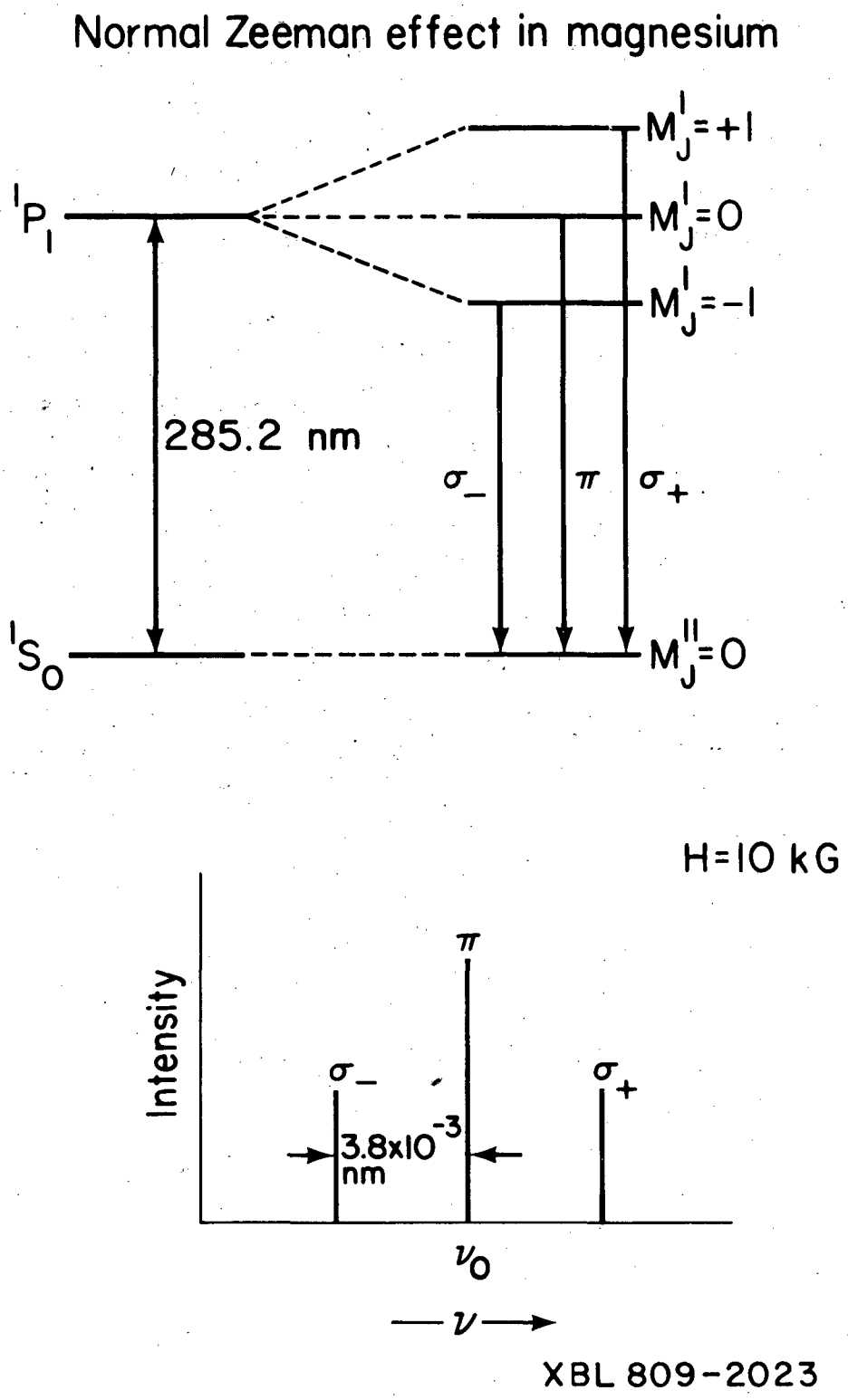
Normal Zeeman effect in magnesium
$^1P_1$
$M_J^1=+1$
$M_J^1=0$
$M_J^1=-1$
285.2 nm
σ_-
π
σ_+
$^1S_0$
$M_J^{11}=0$
H=10 kG
Intensity
π
σ_-
σ_+
3.8×10^{-3} nm
ν_0
ν
XBL 809-2023

FIGURE 1.

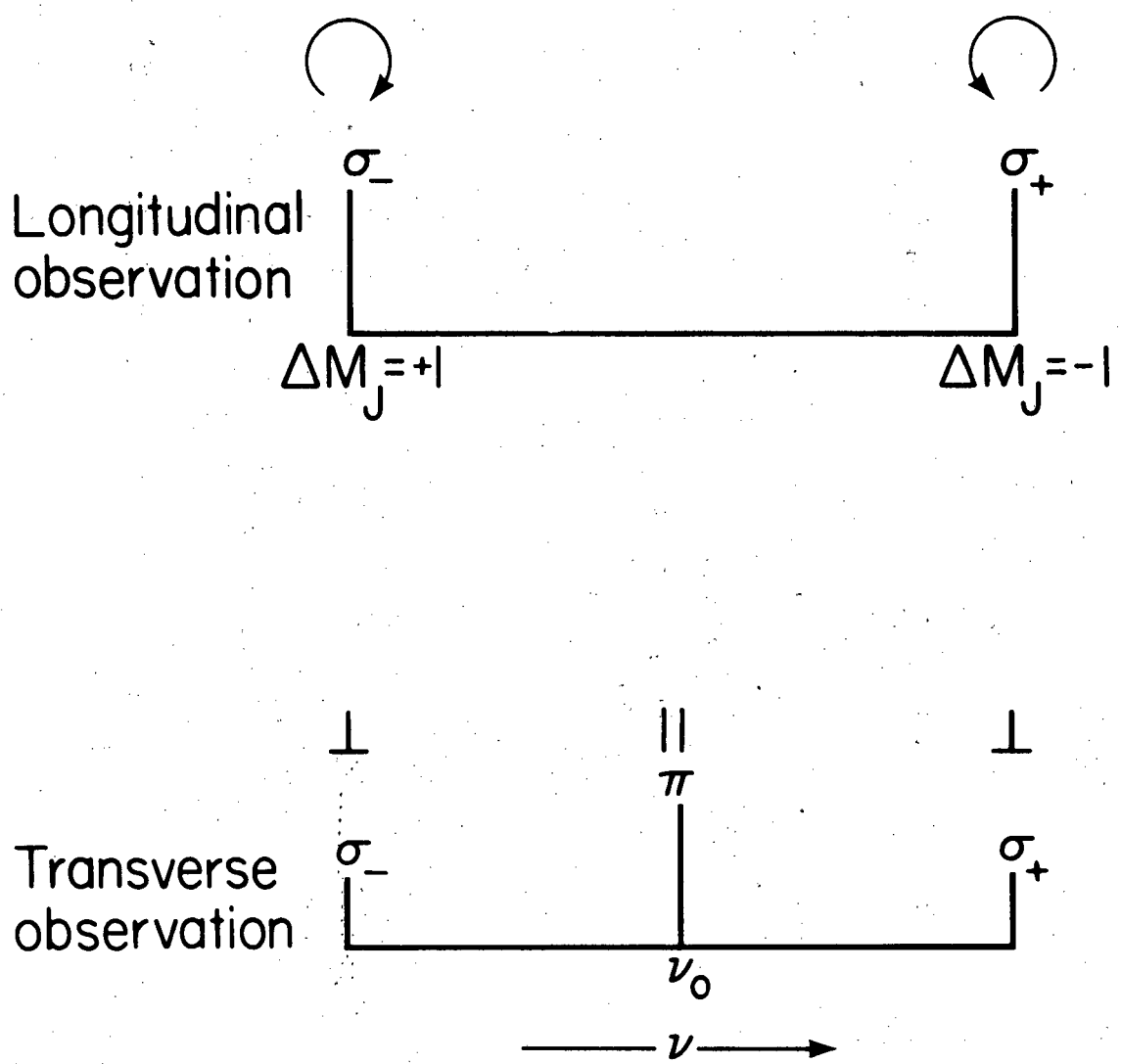

XBL 809-2030

FIGURE 2.

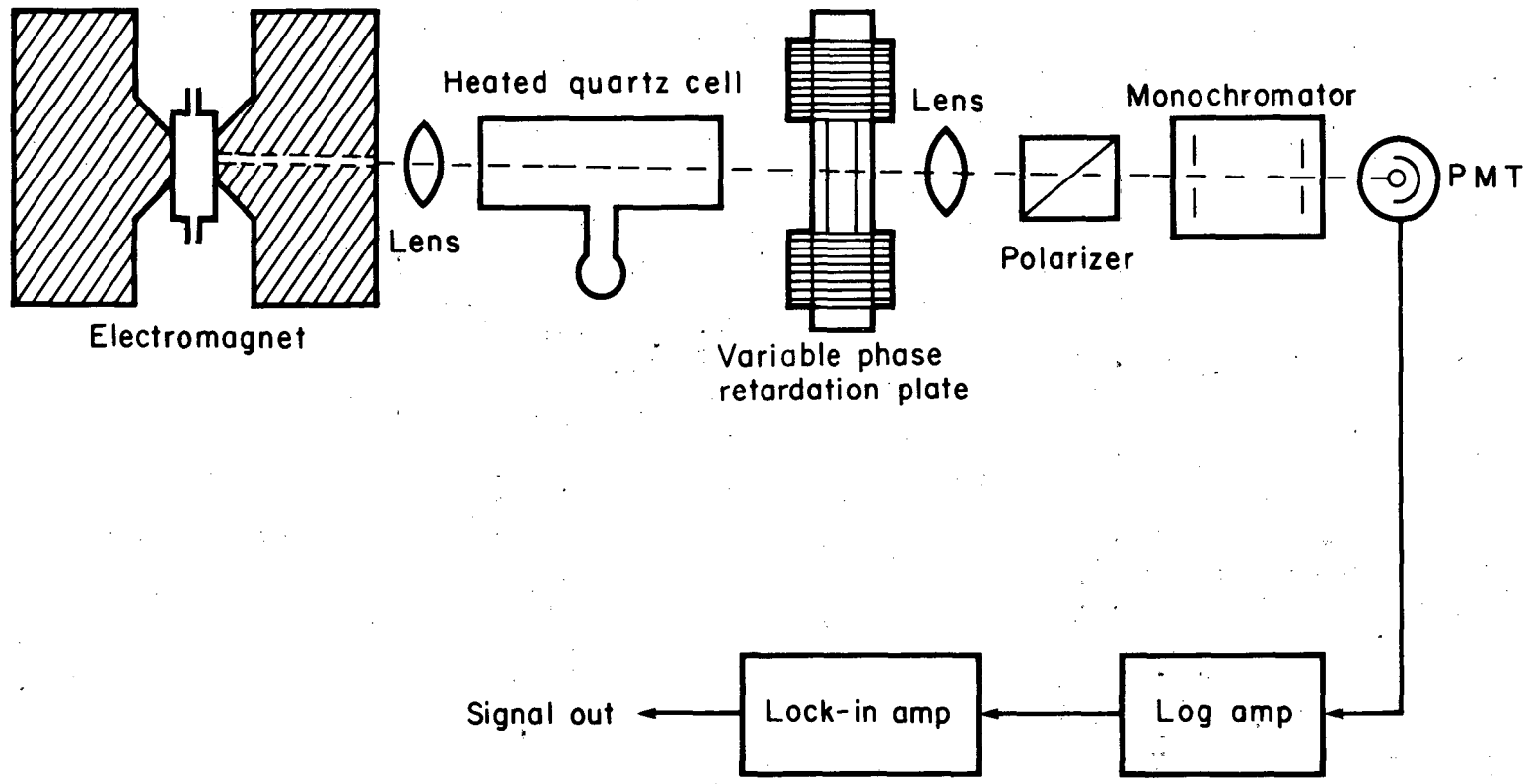

XBL 809-2027

FIGURE 3.

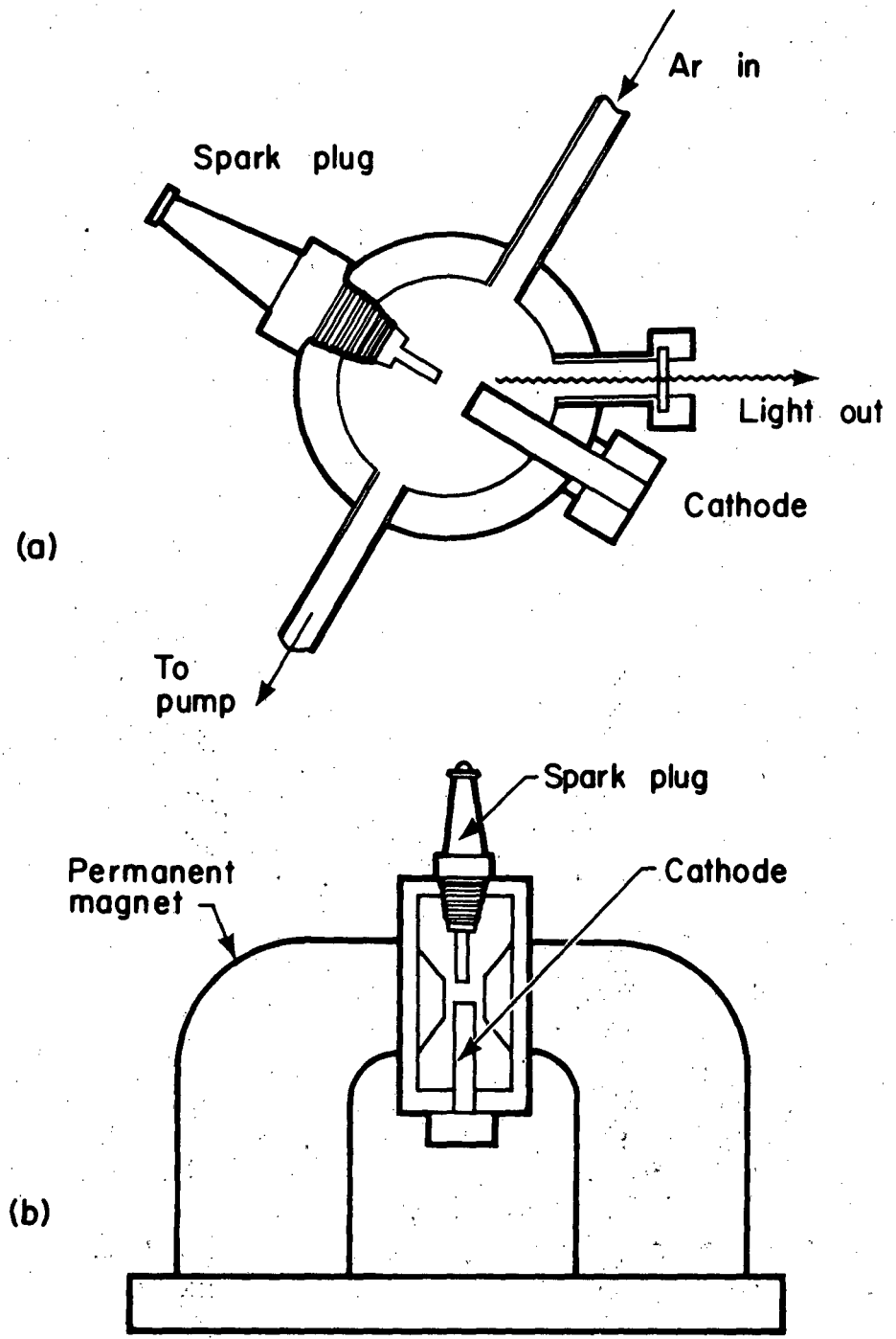

XBL809-2039

FIGURE 4.

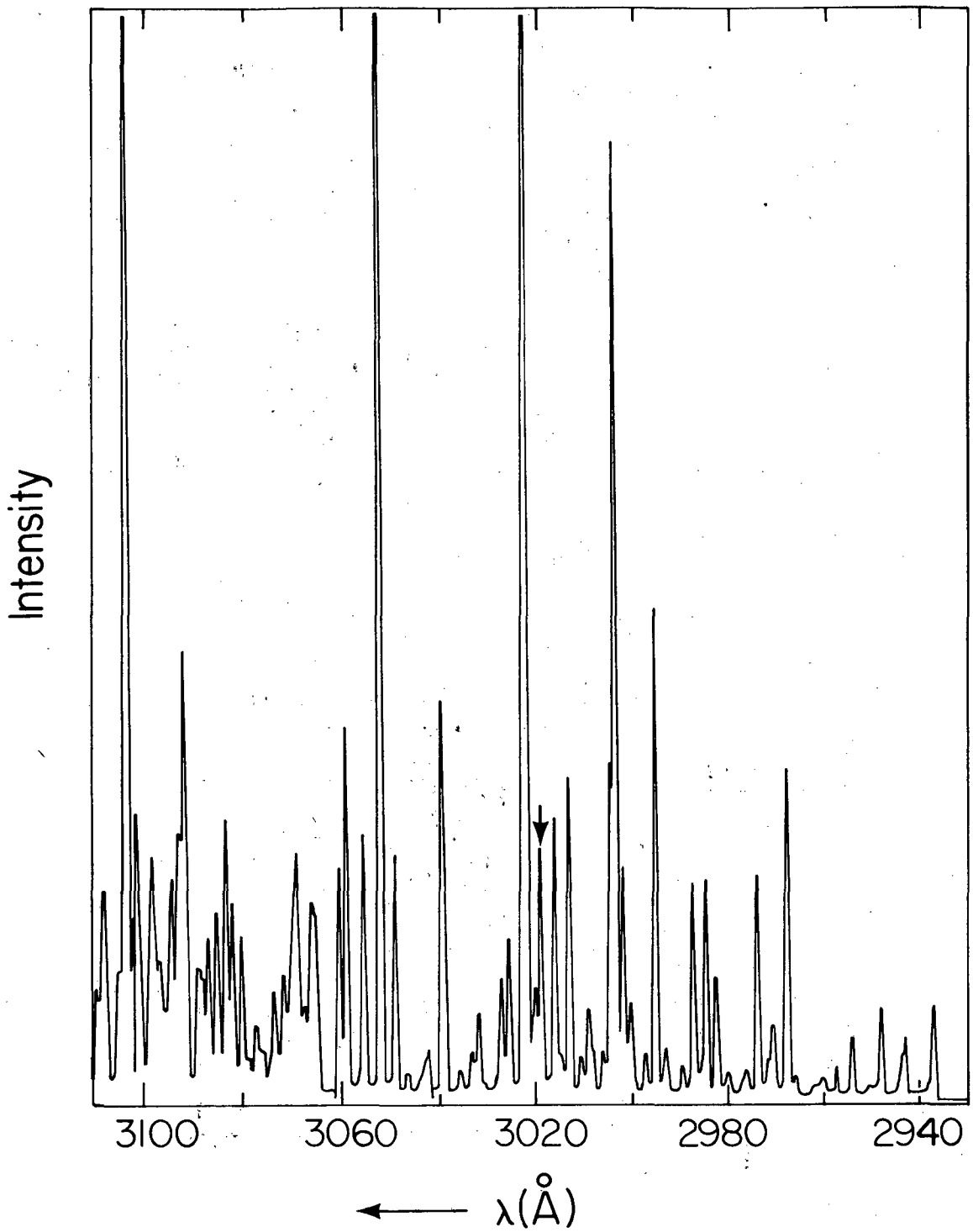

XBL809-2040

FIGURE 5.

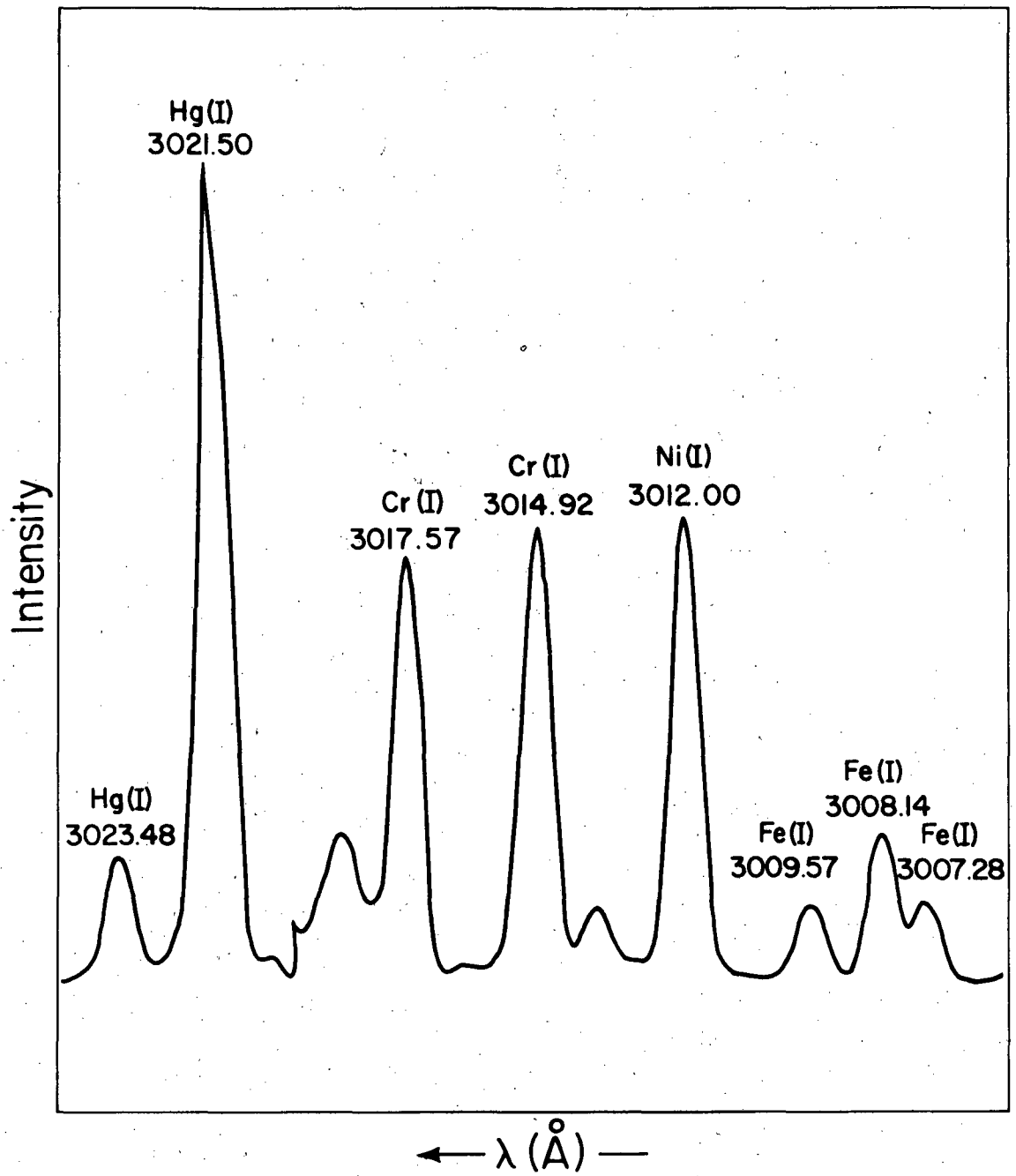

XBL809-2026

FIGURE 6.

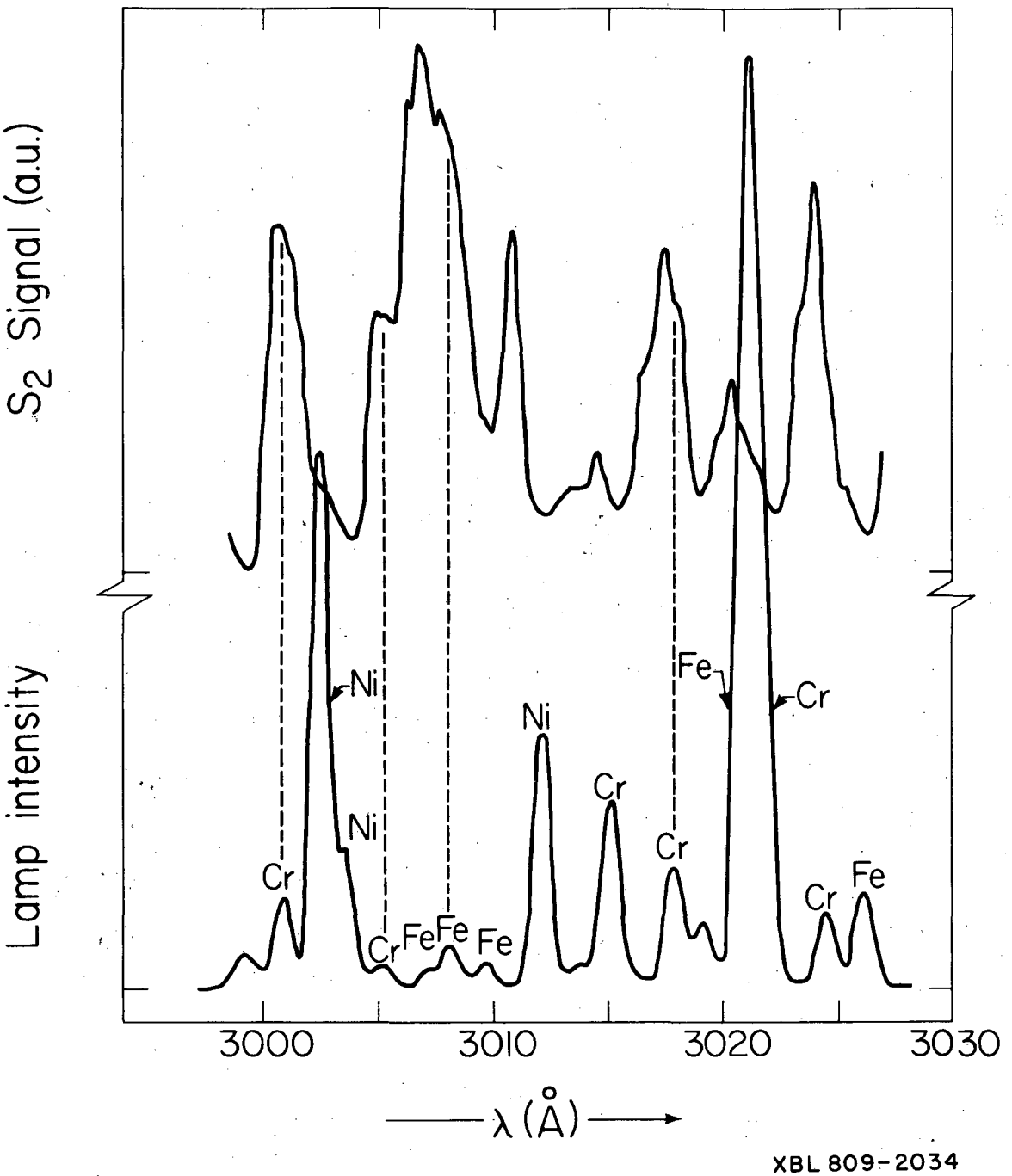

XBL 809-2034

FIGURE 7.

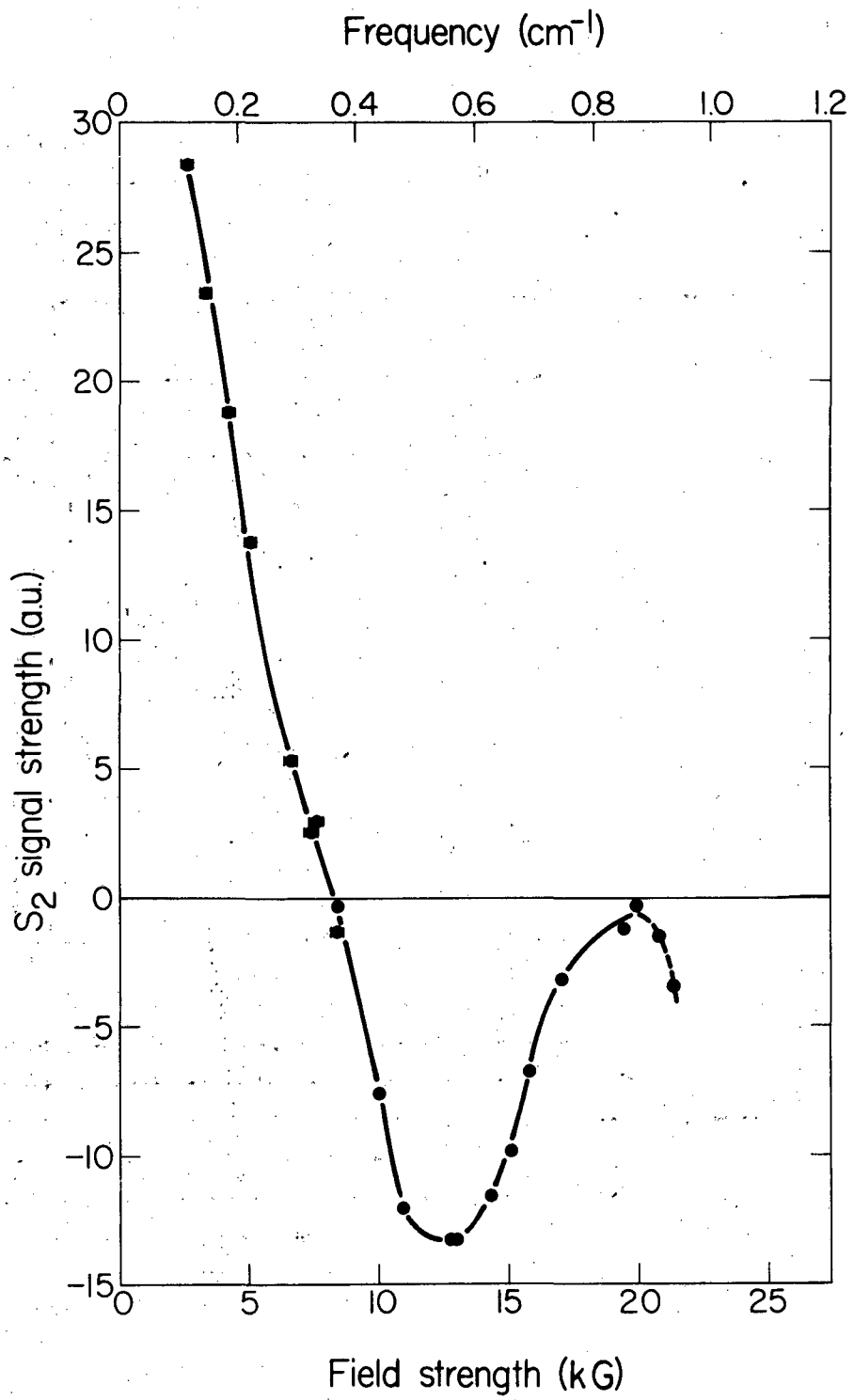

XBL809-2038

FIGURE 8

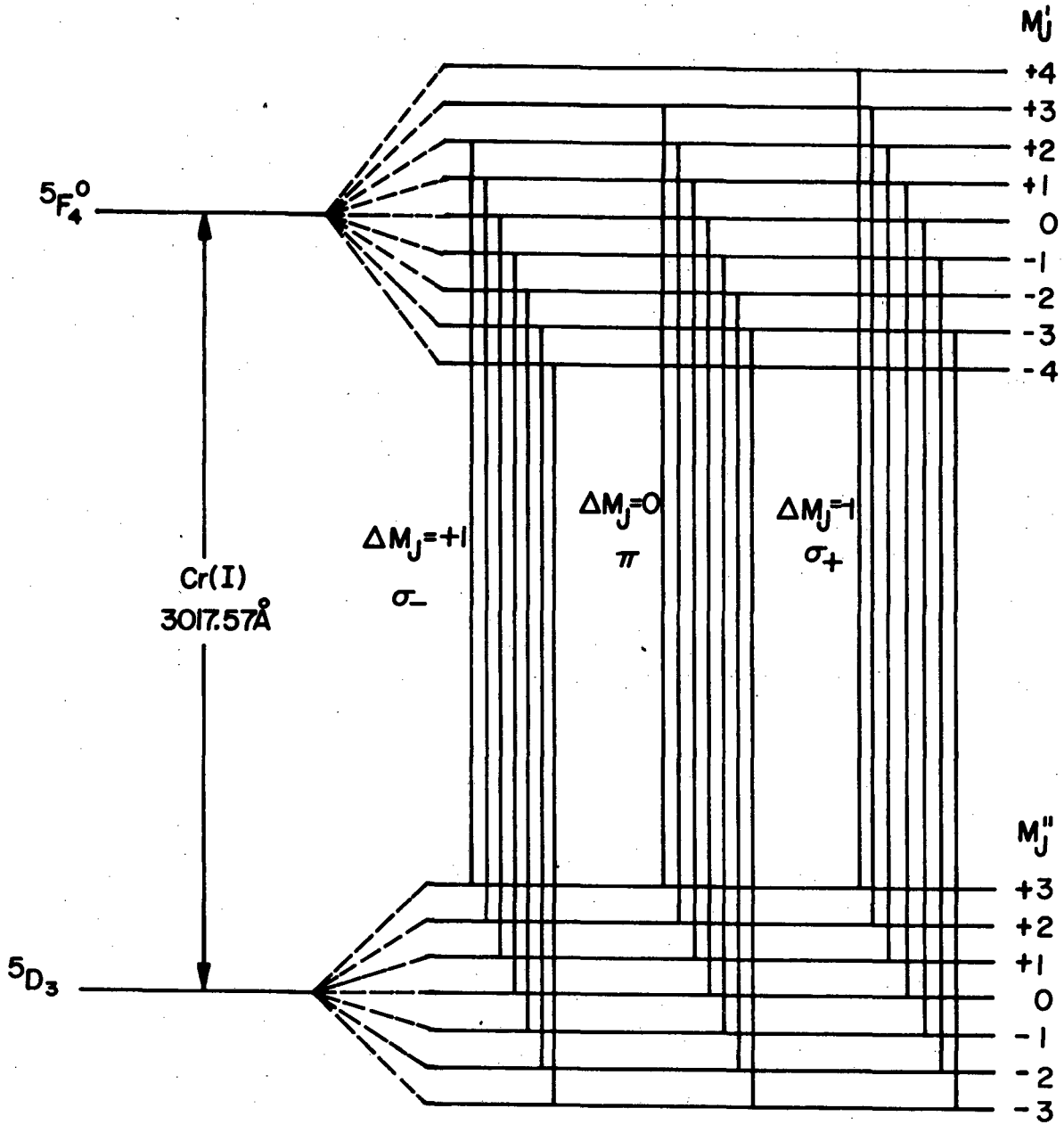

XBL 8010-12263

FIGURE 9.

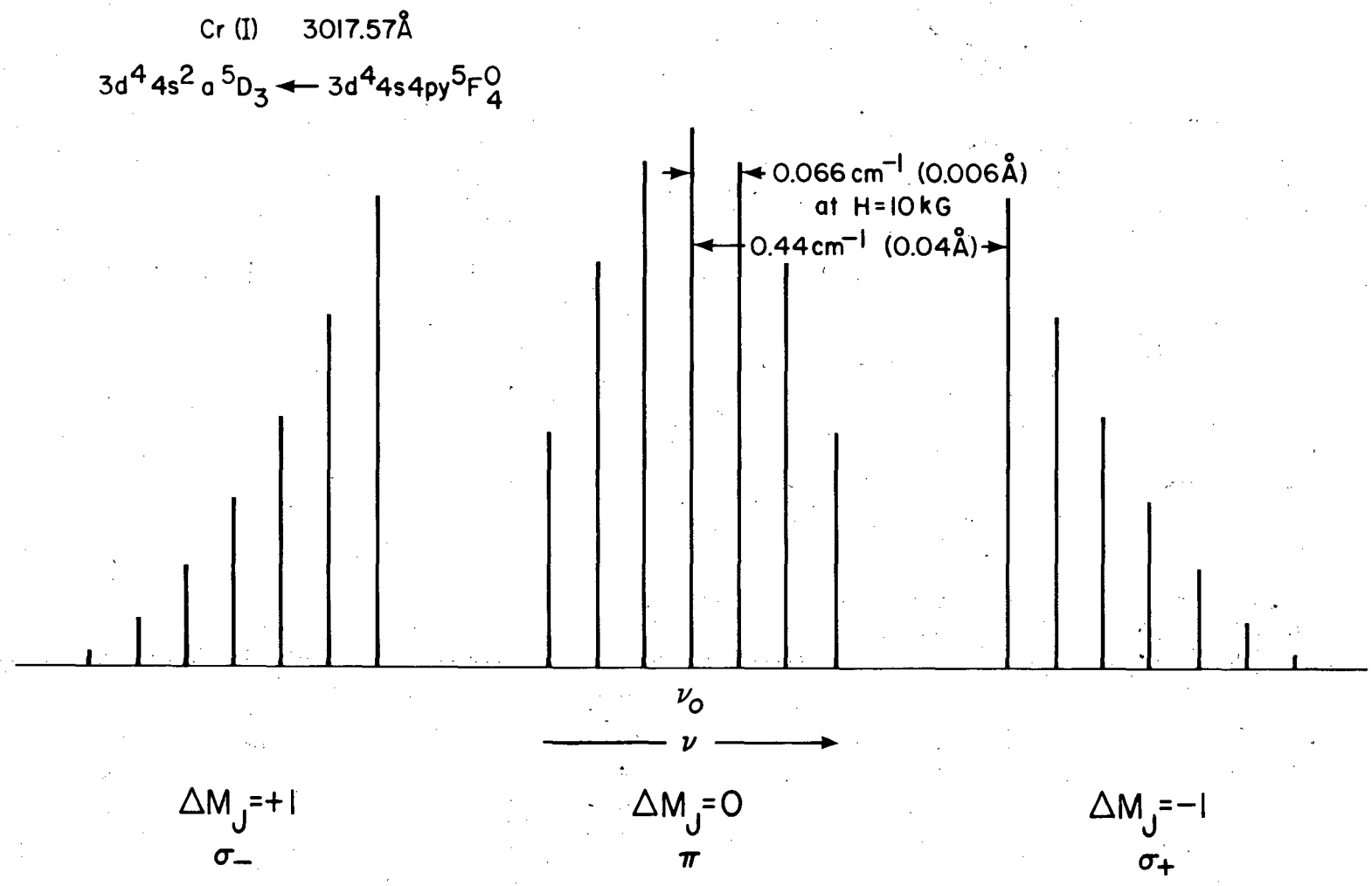

FIGURE 10.

XBL 809-2025

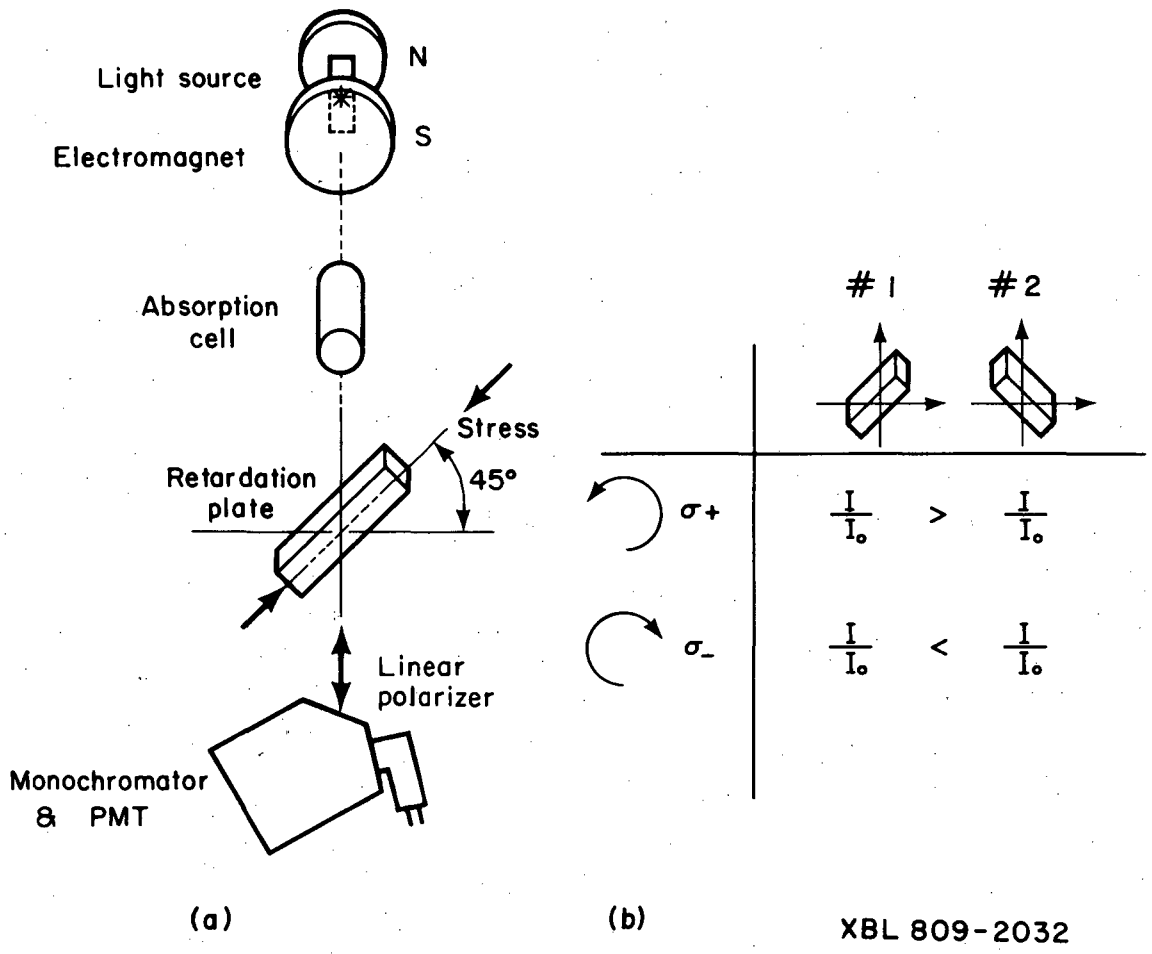
Light source
N
S
Electromagnet
Absorption cell
Stress
45°
Retardation plate
Linear polarizer
Monochromator & PMT
(a)
#1
#2
σ+
σ-
I/I₀ > I/I₀
I/I₀ < I/I₀
(b)
XBL 809-2032

FIGURE 11.

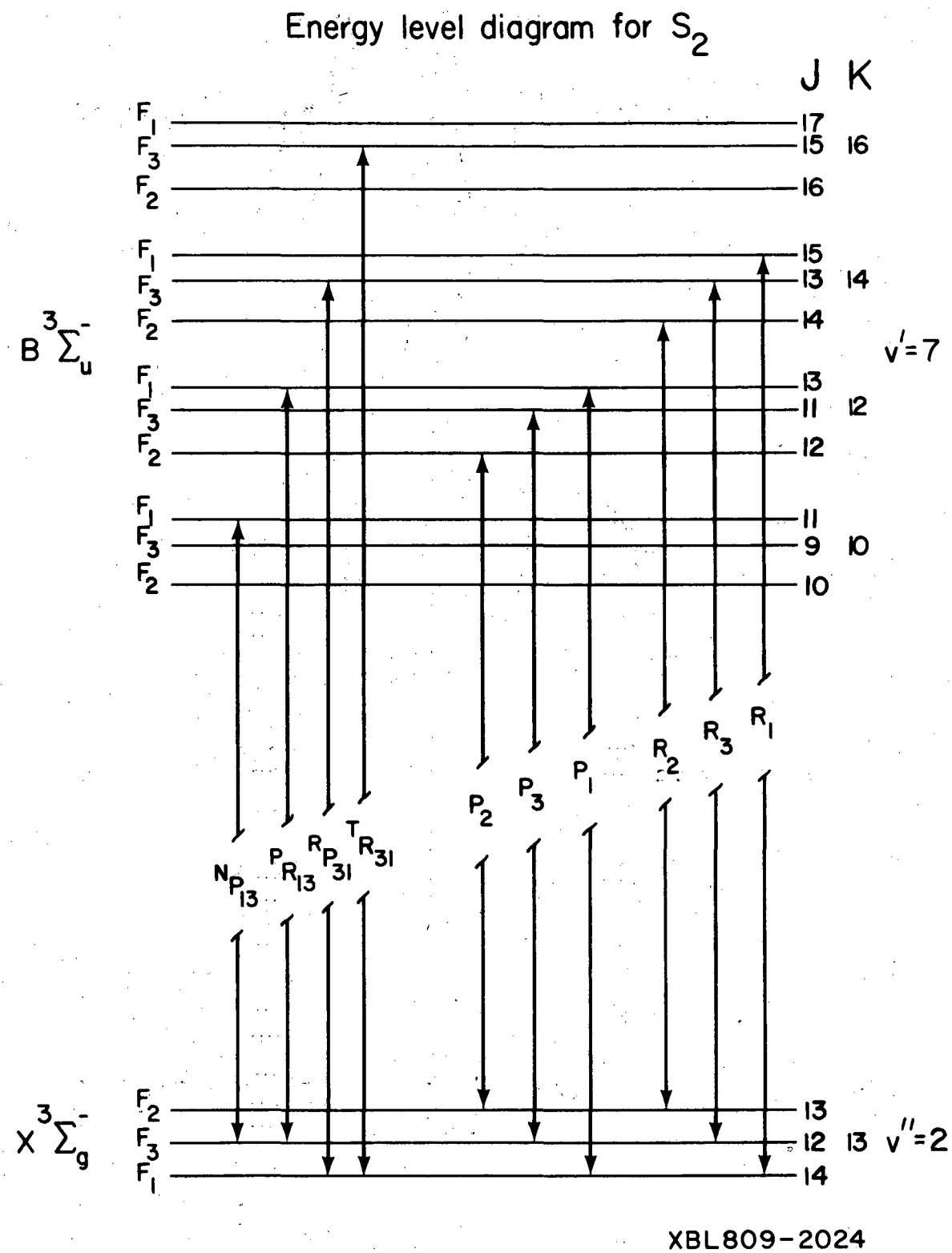
Energy level diagram for S_2
J K
$B^3\Sigma_u^-$
$X^3\Sigma_g^-$
F_1
F_3
F_2
17
15 16
16
15
13 14
14
13
11 12
12
11
9 10
10
13
12 13
14
$v'=7$
$v''=2$
$N_{P_{13}}$
$P_{R_{13}}$
$R_{P_{31}}$
$T_{R_{31}}$
P_2
P_3
P_1
R_2
R_3
R_1
XBL809-2024

FIGURE 12.

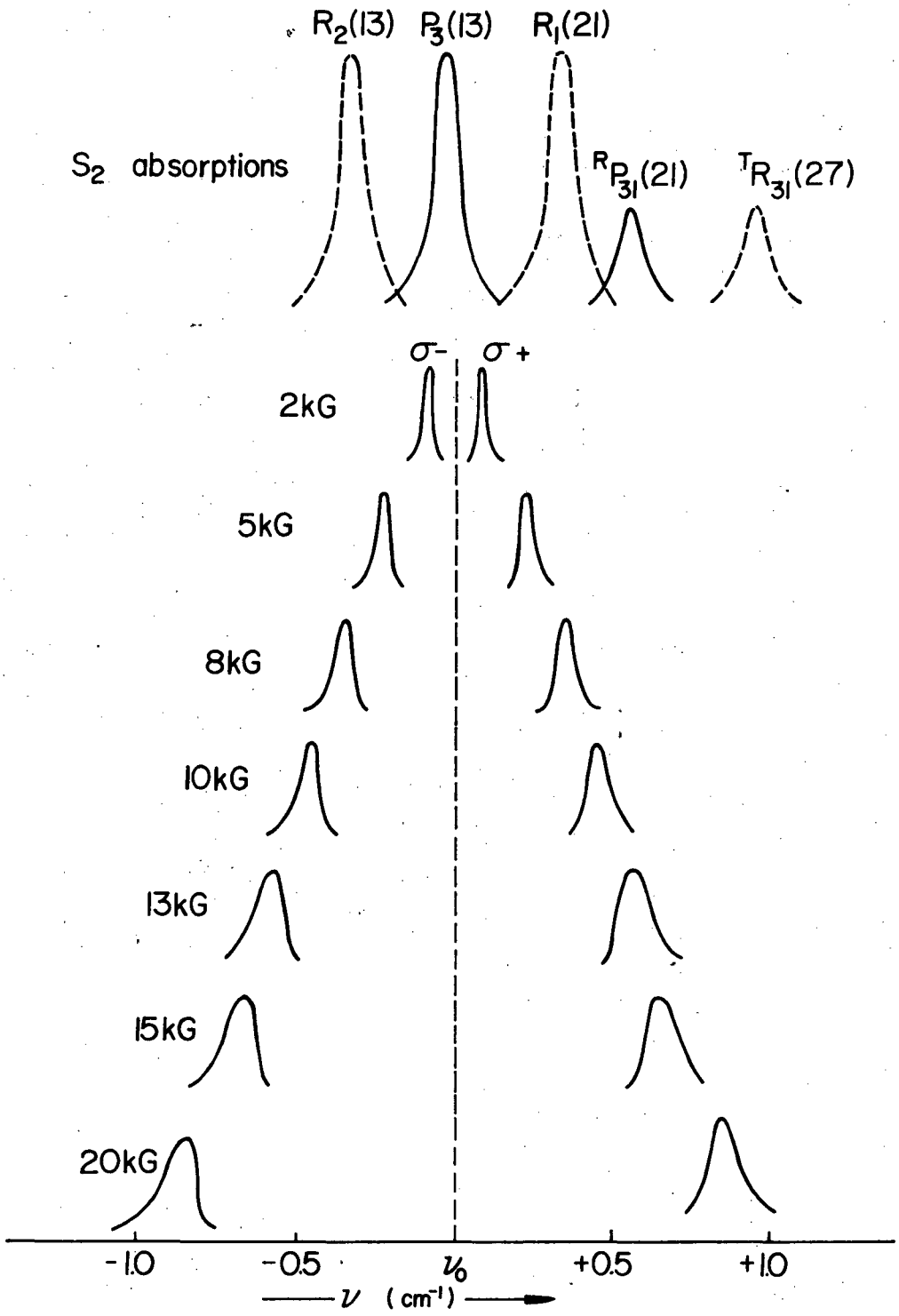

XBL 809-2031

FIGURE 13.

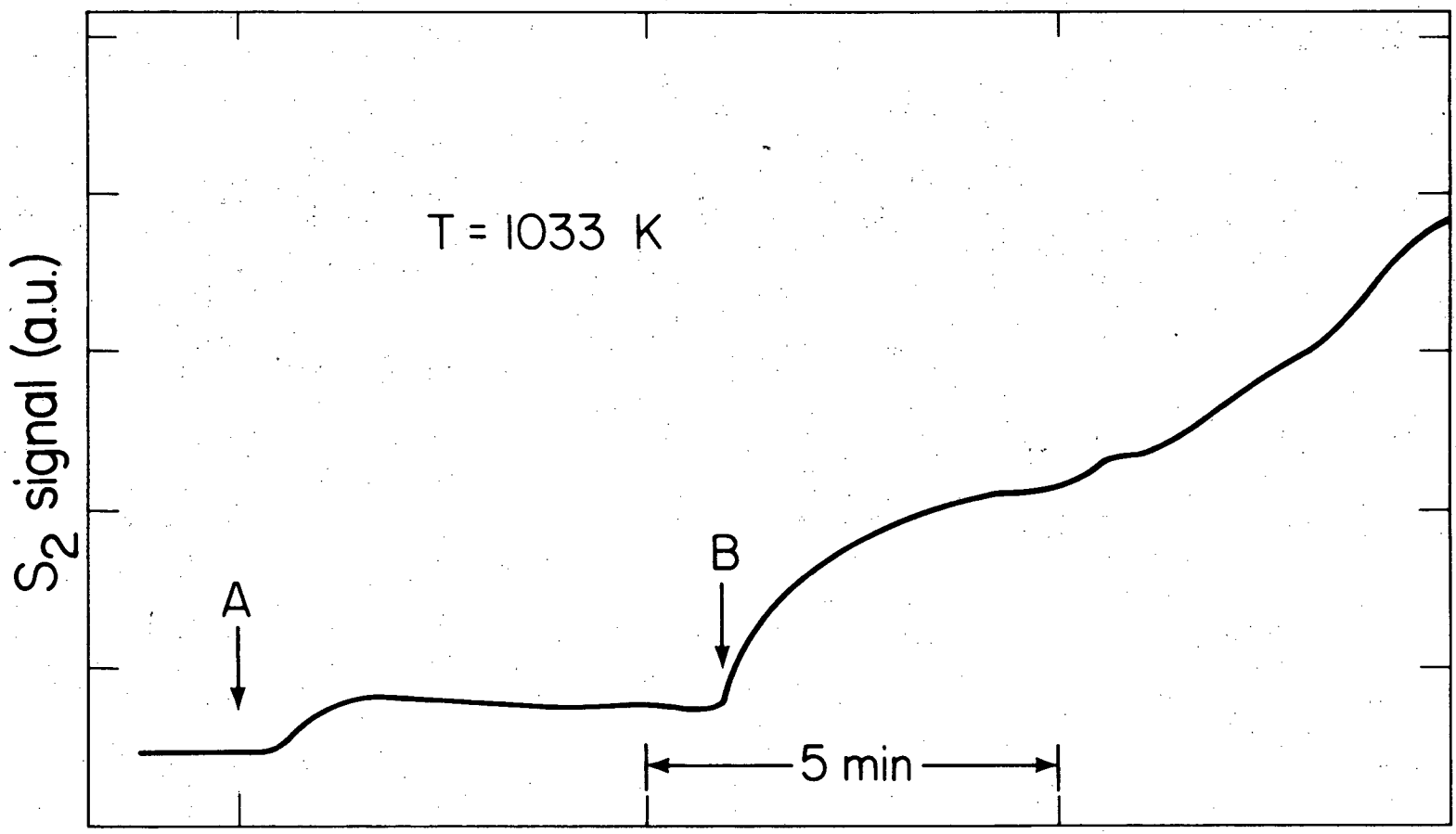

FIGURE 14.

XBL 809-2035

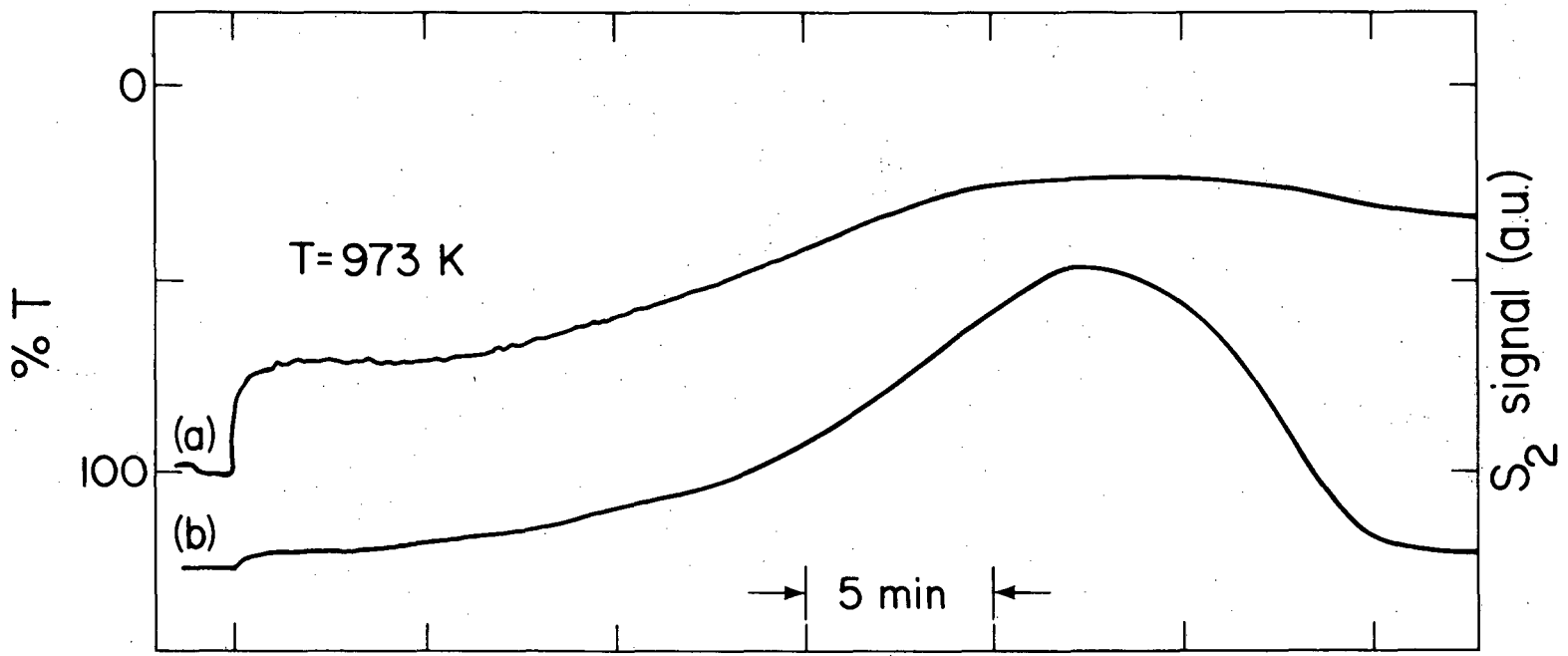

XBL 809-2029

FIGURE 15.

This report was done with support from the Department of Energy. Any conclusions or opinions expressed in this report represent solely those of the author(s) and not necessarily those of The Regents of the University of California, the Lawrence Berkeley Laboratory or the Department of Energy.

Reference to a company or product name does not imply approval or recommendation of the product by the University of California or the U.S. Department of Energy to the exclusion of others that may be suitable.

TECHNICAL INFORMATION DEPARTMENT
LAWRENCE BERKELEY LABORATORY
UNIVERSITY OF CALIFORNIA
BERKELEY, CALIFORNIA 94720